

# Inhibition of Urease by Hydroquinones: A Structural and Kinetic Study

Luca Mazzei,<sup>\*,[a]</sup> Michele Cianci,<sup>[b]</sup> and Stefano Ciurli<sup>[a]</sup>

**Abstract:** Hydroquinones are a class of organic compounds abundant in nature that result from the full reduction of the corresponding quinones. Quinones are known to efficiently inhibit urease, a Ni<sup>II</sup>-containing enzyme that catalyzes the hydrolysis of urea to yield ammonia and carbonate and acts as a virulence factor of several human pathogens, in addition to decreasing the efficiency of soil organic nitrogen fertilization. Here, we report the molecular characterization of the inhibition of urease from *Sporosarcina pasteurii* (SPU) and

*Canavalia ensiformis* (jack bean, JBU) by 1,4-hydroquinone (HQ) and its methyl and *tert*-butyl derivatives. The 1.63-Å resolution X-ray crystal structure of the SPU-HQ complex discloses that HQ covalently binds to the thiol group of  $\alpha$ Cys322, a key residue located on a mobile protein flap directly involved in the catalytic mechanism. Inhibition kinetic data obtained for the three compounds on JBU reveals the occurrence of an irreversible inactivation process that involves a radical-based autocatalytic mechanism.

## Introduction

Quinones are a class of organic compounds containing a fully conjugated cyclic dione structure and represented by archetypical members such as 1,4-benzoquinone (also called *para*-benzoquinone, *p*-BQ) and 1,2-benzoquinone (*o*-BQ). Quinones and their derivatives have been reported as the principal class of molecules present in the interstellar dust observed onboard the NASA spacecraft STARDUST, indicating that they are among the oldest organic compounds in the universe.<sup>[1]</sup> The benzoquinone/semiquinone/hydroquinone (BQ/SQ<sup>•-</sup>/H<sub>2</sub>Q) triad presents unique redox features that make it a vital player as a one- and two-electron acceptor/donor in many redox systems in biology, serving for the movement of electrons in cell compartments, as well as through cells and tissues. For example, coenzyme Q (ubiquinone) and plastoquinone serve as electron and proton transfer for aerobic respiration<sup>[2]</sup> and photosynthesis,<sup>[3]</sup> respectively. A quinone moiety (in the form of naphthoquinone derivative) is also present as a functional group in vitamin K. Quinones are constituents of natural organic matter (NOM), acting as structural components of humic substances in soils<sup>[4]</sup> derived from the microbially mediated lignin degradation and

found in river-derived NOM.<sup>[5]</sup> A large variety of naturally occurring quinones are also produced by bacteria, fungi, plants, and insects.<sup>[6]</sup> Many molecules containing quinone functionalities are exuded by microorganisms and plants in soils to diminish the growth, or kill off their competitors, and have been hypothesized to act by disrupting their electron transfer systems.<sup>[7]</sup> Microorganisms and plants also use quinones for nutrient acquisition, releasing quinone-based compounds to reductively dissolve Fe<sup>III</sup> minerals under iron-deficient conditions.<sup>[8]</sup>

Hydroquinone (HQ), namely the fully reduced form of *p*-BQ, naturally occurs in several plants both as a free molecule and arbutin (hydroquinone  $\beta$ -D-glucopyranoside) and therefore may be found in many consumer products, such as vegetables, fruits, grains, coffee, tea, beer, and wine.<sup>[9]</sup> HQ has been used in skin lightening and clinical formulations for at least 50 years.<sup>[10]</sup> While European Union has limited the use of HQ in over-the-counter formulations since 2000,<sup>[11]</sup> HQ is generally considered a harmless substance<sup>[12]</sup> and prescription-based medications containing HQ are available in European Union countries as well as in many other countries worldwide. The aforementioned HQ analogue arbutin, that is abundantly found in plant extracts of bearberry (*Uvae ursi*), is used in cosmetics and other botanical preparations for skin application.<sup>[13]</sup> Quinones and hydroquinones moieties are also present in other cosmetics, such as hair dyes and products for coating fingernails as well as in chemotherapy compounds, such as doxorubicin (sold under the brand name Adriamycin among others).<sup>[14]</sup>

Quinones and hydroquinones are among the first reported efficient inhibitors of urease<sup>[15]</sup> (urea amidohydrolase, EC 3.5.1.5), a nonredox multimeric enzyme featuring a bimetallic Ni<sup>II</sup>-containing reaction site<sup>[16]</sup> (Figure 1), widespread in nature among fungi, plants, algae and bacteria<sup>[17]</sup> (but not present in mammals), and able to catalyze the hydrolysis of urea to yield ammonia and carbonate.<sup>[16,18]</sup> Urease is standing as an emerging enzymatic target because the products of the overall hydrolytic

[a] L. Mazzei, S. Ciurli  
Laboratory of Bioinorganic Chemistry  
Department of Pharmacy and Biotechnology (FaBiT)  
University of Bologna  
Viale Giuseppe Fanin 40, 40127 Bologna (Italy)  
E-mail: luca.mazzei2@unibo.it

[b] M. Cianci  
Department of Agricultural, Food and Environmental Sciences  
Polytechnic University of Marche  
Via Breccia Bianche 10, 60131 Ancona (Italy)

© 2022 The Authors. Chemistry - A European Journal published by Wiley-VCH GmbH. This is an open access article under the terms of the Creative Commons Attribution Non-Commercial NoDerivs License, which permits use and distribution in any medium, provided the original work is properly cited, the use is non-commercial and no modifications or adaptations are made.

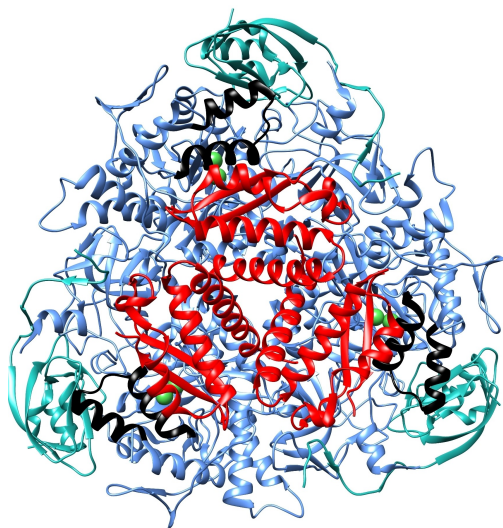


**Figure 1.** Ribbon scheme of native *S. pasteurii* urease; chains  $\alpha$ ,  $\beta$ , and  $\gamma$  of each trimer are colored light blue, green, and red, respectively. The  $\text{Ni}^{\text{II}}$  ions in the active sites of each trimer are shown as green spheres, while the mobile flap regions covering the active site cavities (residues 310–340 of each  $\alpha$  chain) are colored black.

reaction cause an abrupt increase in pH of the environment that in turn negatively affects medical and pharmaceutical,<sup>[19]</sup> as well as agricultural and environmental settings.<sup>[20]</sup> Indeed urease is exploited as a virulence factor by several microbial human pathogens,<sup>[21]</sup> many of which have been included by the World Health Organization among microbes presenting high antibiotic-resistance phenomena and for which the research and development of new antibiotics is urgently needed.<sup>[22]</sup> Moreover, the wide spreading of urease in soils determines the release of large amounts of gaseous ammonia in the atmosphere upon use of urea-based fertilizers. This causes, on one side, a decreased efficiency of nitrogen soil fertilization and, on the other, an increase of airborne particulate matter (PM) that significantly contributes to atmospheric pollution.<sup>[23]</sup>

A recent integrated study has been performed shedding light on the inhibition mode of *p*-BQ on urease from the ureolytic soil bacterium *Sporosarcina pasteurii* (SPU), at the molecular level.<sup>[24]</sup> Urease inhibition by *p*-BQ occurs through an irreversible process of the first order with respect to both SPU and BQ that leads to an inactive form of SPU. The structural details of such inhibition have been disclosed by the X-ray crystal structure of SPU co-crystallized in the presence of *p*-BQ: the ligand covalently binds to the thiol  $\text{S}_{\gamma}$  atom of a conserved cysteine residue ( $\alpha\text{Cys322}$  following SPU numbering), the latter belonging to a 30-residue flexible helix-turn-helix motif (also called mobile flap; Figure 1) located at the entrance of the dinickel containing active site cavity and extensively proven to be directly involved in the catalytic mechanism of urease by switching from an open to a closed state.<sup>[16c,25]</sup> In this context, the covalent adduct originated upon the binding of *p*-BQ on  $\alpha\text{Cys322}$  reduces the conformational flexibility of the mobile flap, in turn blocking the enzymatic activity.<sup>[24]</sup> A geometric analysis of the adduct also suggested the ligand in its final

oxidation state is the fully reduced HQ, an observation consistent with a mechanism involving a Michael addition of the cysteine thiol on the original *p*-BQ scaffold.

Even though a broad family of urease inhibitors which directly bind to the  $\text{Ni}^{\text{II}}$  ions in the active site has been characterized in the past decades,<sup>[16c,18c]</sup> an ever-growing number of ligands are emerging that share with *p*-BQ the ability of inactivating urease by blocking the mobility of the active site flap, including, among the others, catechol (CAT)<sup>[26]</sup> and its derivatives,<sup>[27]</sup> as well as heavy transition metal ions, such as silver(I)<sup>[28]</sup> and gold(I).<sup>[29]</sup> Considering that *p*-BQ has been also reported to inhibit intracellular urease in vivo experiments,<sup>[30]</sup> and given the presence, in the living cells, of a reducing environment that would facilitate the presence of HQs in their fully reduced form, the aim of the present work has been to provide a molecular characterization for the inhibition of urease by HQ, comparing the obtained results with the reported data for the inhibition of oxidized *p*-BQ on the enzyme. The X-ray crystal structure of SPU was reported at 1.63 Å resolution and HQ is found covalently bound to the conserved mobile flap  $\alpha\text{Cys322}$  residue, structurally retracing the mode of binding previously reported for *p*-BQ on urease.<sup>[24]</sup> In addition, a kinetic study on the inhibition of *Canavalia ensiformis* (jack bean) urease (JBU; largely homologous to SPU) by HQ and two derivatives, namely methyl-hydroquinone (MHQ) and *tert*-butyl-hydroquinone (tBHQ), revealed a shared time-dependent inhibition process that, unlike what previously reported for *p*-BQ, is governed by the oxidation of the testing ligands by molecular oxygen into molecular species reactive towards urease.

## Experimental Section

**Enzymes and reagents preparation:** Pure *S. pasteurii* urease (molar mass = 250 kDa) was obtained from *S. pasteurii* DSM 33 bacterial cells as previously reported,<sup>[31]</sup> concentrated up to 11 mg mL<sup>-1</sup> of active protein and stored at +4 °C in 50 mM HEPES buffer, 150 mM NaCl, 50 mM Na<sub>2</sub>SO<sub>3</sub> and 2 mM EDTA, at pH 7.5, for crystallographic purposes. *C. ensiformis* (jack bean) urease (molar mass = 550 kDa) type C-3, powder ( $\geq 600\,000$  units per g) was purchased from Merck (Milan, Italy), dissolved at a final concentration of 50  $\mu\text{g mL}^{-1}$  of active protein in 20 mM HEPES buffer, at pH 7.5, stored at -80 °C as stock aliquots and used for kinetic studies. Activity quantification of both the enzymes was carried out using a pH-STAT method<sup>[32]</sup> by considering specific activities of 2.5 and 3.5 U  $\mu\text{g}^{-1}$  for SPU and JBU, respectively.<sup>[15h]</sup>

Benzene-1,4-diol [hydroquinone, HQ], 2-methylbenzene-1,4-diol [methylhydroquinone, MHQ] and 2-*tert*-butylbenzene-1,4-diol [*tert*-butylhydroquinone, tBHQ] were purchased from Merck (Milan, Italy) and properly handled and dissolved depending on the analysis to be carried out (see below for details).

**Crystallization, data collection and structural determination:** A 100- $\mu\text{L}$  aliquot of 11 mg mL<sup>-1</sup> SPU was diluted down to 1 mg mL<sup>-1</sup> and buffer-exchanged through successive dilution-concentration cycles using Amicon Ultra centrifugal filter units-MWCO 10 kDa (Merck) and 50 mM HEPES buffer, 150 mM NaCl, and 2 mM EDTA, at pH 7.5 (crystallization buffer), to decrease Na<sub>2</sub>SO<sub>3</sub> concentration (present at 50 mM in the storage buffer of the enzyme) down to values lower than 20  $\mu\text{M}$ . The buffer-exchanged SPU solution was split in three aliquots. Stock solutions of the three inhibitors, at a

concentration of 10 mM, were prepared in the crystallization buffer and added 1:5 (v/v) to the three SPU solutions, thus obtaining enzyme solutions incubated in the presence of 2 mM ligand. After a proper incubation period, during which the enzyme activity was abolished (ca. 1–3 hours), each SPU-inhibitor mixture was concentrated up to 11 mg mL<sup>-1</sup>. Crystallization trials were set up mixing 1.5 μL of the SPU-inhibitor solution with an equal volume of precipitant [1.6–2.0 M (NH<sub>4</sub>)<sub>2</sub>SO<sub>4</sub> dissolved in 50 mM sodium citrate buffer, pH 6.3] and equilibrating the resulting crystallization drops through vapor diffusion (hanging-drop method) at 293 K against 0.5 mL of the precipitant solution using EasyXtal 15-Well plates (Quiagen, Hilden, Germany). As no inhibitor was present in the precipitant solution, crystallization occurred in the presence of 1 mM ligand.

Rice-shaped protein crystals (dimensions up to 0.1 × 0.1 × 0.3 mm<sup>3</sup>) typically grew in a broad interval of (NH<sub>4</sub>)<sub>2</sub>SO<sub>4</sub> concentrations after 1–2 weeks. Crystals were cryoprotected by transferring them in a solution containing 50 mM citrate buffer at pH 6.3, 2.4 M (NH<sub>4</sub>)<sub>2</sub>SO<sub>4</sub>, and 20% (v/v) ethylene glycol, and then flash-cooled and stored in liquid nitrogen.

Diffraction data were collected at 100 K using synchrotron X-ray radiation at the EMBL P13 beamline of the Petra III storage ring, c/o DESY, Hamburg (Germany).<sup>[33]</sup> Helical scanning was performed to minimize radiation damage and achieve higher data quality. Data processing and reduction were carried out using XDS<sup>[34]</sup> and AIMLESS.<sup>[35]</sup> The crystals belonged to space group *P*<sub>6</sub><sub>3</sub><sub>2</sub><sub>2</sub>, isomorphous with all the crystal structures of SPU determined so far. The X-ray crystal structure of SPU bound to catechol (PDB ID: 5G4H, 1.50 Å resolution),<sup>[26]</sup> devoid of solvent molecules and ligands, and after coordinates randomization, was used as a starting model to obtain the initial phases for the structure determination. Restrainted refinement was carried out using REFMAC5<sup>[36]</sup> and isotropic atomic displacement parameters (ADPs) (including the hydrogen atoms in the riding positions). Manual model rebuilding, as well as water or ligand addition/inspection were conducted using COOT.<sup>[37]</sup> Unbiased omit electron density maps for nonproteinaceous ligands were calculated using Fourier coefficients  $F_o - F_c$  and phases from the last cycle of refinement before ligand addition to the refining model. Given the poor quality of the electron density maps obtained in the cases of SPU co-crystallized in the presence of MHQ and tBHQ, only the refinement and model building for the data collected on SPU co-crystallized in the presence of HQ were finalized, the X-ray crystal structure was determined at a final resolution of 1.63 Å, and the resulting structure factors and atomic coordinates were deposited in the Protein Data Bank with the accession code 8A18. Data collection and final refinement statistics are given in Table 1. Figures were generated by using PyMol (The PyMOL Molecular Graphics System, v. 2.4.1, Schrödinger, LLC).

**Kinetic measurements:** Pre-incubation experiments were conducted at 25 °C as previously described.<sup>[24,26,27]</sup> In brief, a solution of 50 μg mL<sup>-1</sup> active JBU dissolved in 20 mM HEPES buffer, pH 7.5, was 100-fold diluted in Cresol Red (CR) buffer, consisting of 30 mg L<sup>-1</sup> CR dissolved in 2 mM HEPES buffer (pH 7.5), 2 mM EDTA. In the case of HQ and MHQ, they were dissolved in CR buffer at 10 mM and then added at the desired working concentration (0.2, 0.4, 0.8, and 1.6 mM) onto the enzyme reaction mixture, while due to lower solubility of tBHQ, incubation mixtures for the latter were prepared by directly dissolving the proper amount of powder in CR buffer and then adding JBU to it; in any case, the time when the enzyme and the inhibitor were mixed were taken as zero time of incubation. After appropriate time intervals, enzyme-inhibitor aliquots were withdrawn from the incubation mixture, 100 mM urea was added and the change in absorbance at 573 nm, due to cresol red change in color from yellow to purple, was spectrophotometrically monitored over one minute reaction time using a Cary 60 UV-Vis

**Table 1.** X-ray diffraction data collection, processing, and refinement statistics.

Data collection	8A18
wavelength [Å]	0.9537
detector	Dectris Pilatus 6 M
crystal-to-detector distance [mm]	327.64
oscillation angle [°]	0.100
number of images	1200
space group	<i>P</i> <sub>6</sub> <sub>3</sub> <sub>2</sub> <sub>2</sub>
unit cell <i>a</i> , <i>b</i> , <i>c</i> [Å]	131.7, 131.7, 189.1
resolution range [Å] <sup>a</sup>	1.63–114.03 (1.63–1.66)
total number of reflections <sup>[a]</sup>	1961423 (83131)
unique reflections <sup>[a]</sup>	120118 (5878)
multiplicity <sup>[a]</sup>	16.3 (14.1)
completeness <sup>[a]</sup> [%]	100.0 (100.0)
$R_{\text{sym}}^{\text{[a,b]}}$ [%]	12.0 (199.0)
$R_{\text{pim}}^{\text{[a,c]}}$ [%]	4.3 (78.6)
mean <i>I</i> half-set correlation CC(1/2) <sup>[a]</sup>	0.999 (0.685)
mean <i>I</i> / <i>σ</i> <sup>[a]</sup>	19.9 (1.5)
number of monomers in the asymmetric unit	3
$R_{\text{factor}}^{\text{[d]}}$ [%]	12.4
$R_{\text{free}}^{\text{[d]}}$ [%]	15.6
Cruickshank's DPI for coordinate error <sup>[e]</sup> based on $R_{\text{factor}}$ [Å]	0.066
Wilson plot <i>B</i> factor [Å <sup>2</sup> ]	18.2
average all atom <i>B</i> factor <sup>[f]</sup> [Å <sup>2</sup> ]	21.85
<i>B</i> factor <sup>[f]</sup> for the Ni atoms [Å <sup>2</sup> ]	20.7, 19.2
RMS (bonds) <sup>[d]</sup>	0.013
RMS (angles) <sup>[d]</sup>	1.862
total number of atoms	7215
total number of water molecules	666
solvent content [%]	53.25
Matthews coefficient [Å <sup>3</sup> /Da]	2.63
most favored regions [%] <sup>[g]</sup>	90.3
additionally allowed regions [%] <sup>[g]</sup>	9.0
generously allowed regions [%] <sup>[g]</sup>	0.6
disallowed regions [%] <sup>[g]</sup>	0.2

[a] Highest resolution bin in parentheses. [b]  $R_{\text{sym}} = \frac{\sum_{hkl} \sum_j |I_j - \langle I \rangle|}{\sum_{hkl} \sum_j I_j}$ , where *I* is the intensity of a reflection, and  $\langle I \rangle$  is the mean intensity of all symmetry related reflections *j*. [c]  $R_{\text{p.i.m.}} = \frac{\sum_{hkl} \{ [1/(N-1)]^{1/2} \sum_j |I_j - \langle I \rangle| \}}{\sum_{hkl} \sum_j I_j}$ , where *N* is the multiplicity.<sup>[41]</sup> [d] Taken from REFMAC.<sup>[36]</sup>  $R_{\text{free}}$  was calculated using 5% of the total reflections that were randomly selected and excluded from refinement. [e]  $\text{DPI} = R_{\text{factor}} \cdot D_{\text{max}} \cdot \text{compl}^{-1/5} \sqrt{\frac{N_{\text{atoms}}}{(N_{\text{ref}} - N_{\text{params}})}}$ , where  $N_{\text{atoms}}$  is the number of the atoms included in the refinement,  $N_{\text{ref}}$  is the number of the reflections included in the refinement,  $D_{\text{max}}$  is the maximum resolution of reflections included in the refinement, *compl* is the completeness of the observed data, and for isotropic refinement,  $N_{\text{params}} \approx 4N_{\text{atoms}}$ .<sup>[42]</sup> [f] Taken from BAVEGAGE.<sup>[41]</sup> [g] Taken from PROCHECK.<sup>[41]</sup>

Spectrophotometer (Agilent Technologies, CA, USA). All the assays were carried out as independent triplicates and urease activity of each was calculated by a linear fitting of the straight portion in the absorbance versus time curve. The independent fitting results were averaged, normalized with respect to the averaged enzyme activity measured at time zero of incubation, and plotted as a mean percentage ± standard deviation (SD).

## Results and Discussion

To explore the structural aspects of the inhibition mode of HQ, MHQ, and tBHQ on urease, co-crystallization attempts were carried out using SPU. Single crystals were obtained in all cases,

and the corresponding X-ray diffraction data were collected. However, the quality of the electron density maps obtained in the cases of SPU co-crystallized with MHQ and tBHQ were of poor quality, especially concerning the mobile flap region, thus impeding a correct interpretation of the model. The final X-ray crystal structure determined starting from the X-ray diffraction data collected on the SPU-HQ co-crystal displays a  $(\alpha\beta\gamma)_3$  quaternary assembly typical of SPU and other bacterial ureases,

showing very low C $\alpha$  RMSD values calculated with respect to the X-ray crystal structures of SPU in the native form (PDB ID: 4CEU) and co-crystallized in the presence of *p*-BQ<sup>[24]</sup> (PDB ID: 5FSE) for chains  $\alpha$ ,  $\beta$  and  $\gamma$  (Table 2), as well as a completely conserved coordination environment of Ni<sup>II</sup> ions in active site with respect to the same structures (Table 3). In addition, the X-ray crystal structure of SPU co-crystallized in the presence of HQ shares with the previously mentioned structures, as well as with the structure of SPU bound to catechol (CAT,<sup>[24]</sup> PDB ID: 5G4H), also the open conformation of the mobile flap covering the active site.

The unbiased omit electron density map calculated after the successful refinement of the protein backbone and sidechains, as well as the addition of solvent molecules and ions originally present in the crystallization cocktail, revealed the presence of two unmodeled blobs in the vicinity of the thiol groups of the active site mobile flap  $\alpha$ Cys322 and  $\alpha$ Cys555 (Figure 2A,B), another solvent-exposed cysteine residue present in SPU that

**Table 2.** C $\alpha$  RMSD of the crystal structures of SPU bound to HQ calculated with respect to the native urease (PDB ID: 4CEU), as well as urease co-crystallized in the presence of *p*-BQ (PDB ID: 5FSE). All values are reported in Å.

	4CEU (NAT)	5FSE ( <i>p</i> -BQ)
$\alpha$	0.141	0.113
$\beta$	0.122	0.103
$\gamma$	0.098	0.095

**Table 3.** Selected distances and angles around the Ni<sup>II</sup> ions in the crystal structure of SPU bound to HQ and, as a comparison, in that of SPU co-crystallized in the presence of *p*-BQ (PDB ID: 5FSE).

PDB ID <sup>[a]</sup> (ligand)	8A18 (HQ)	5FSE <sup>[b]</sup> ( <i>p</i> -BQ)
Ni–L distances [Å]		
Ni(1)– $\alpha$ Lys220* O01	2.0	2.0
Ni(1)–L <sub>B</sub>	2.1	2.0
Ni(1)–L <sub>1</sub>	2.2	2.3
Ni(1)– $\alpha$ His249 N $\delta$	2.0	2.2
Ni(1)– $\alpha$ His275 N $\epsilon$	2.1	2.2
Ni(2)– $\alpha$ Lys220* O02	2.1	2.1
Ni(2)–L <sub>B</sub>	2.1	2.1
Ni(2)–L <sub>2</sub>	2.1	2.3
Ni(2)– $\alpha$ His137 N $\epsilon$	2.1	2.0
Ni(2)– $\alpha$ His139 N $\epsilon$	2.1	2.3
Ni(2)– $\alpha$ Asp363 O $\delta$ 1	2.1	2.3
Ni(1)–Ni(2)	3.6	3.5
L <sub>1</sub> –L <sub>2</sub>	2.2	2.1
L–Ni–L angles [°]		
$\alpha$ Lys220* O01–Ni(1)– $\alpha$ His249 N $\delta$	101.7	108.5
$\alpha$ Lys220* O01–Ni(1)– $\alpha$ His275 N $\epsilon$	104.8	106.7
$\alpha$ Lys220* O01–Ni(1)–L <sub>B</sub>	96.5	98.1
$\alpha$ Lys220* O01–Ni(1)–L <sub>1</sub>	107.4	108.3
$\alpha$ His249 N $\delta$ –Ni(1)– $\alpha$ His275 N $\epsilon$	95.6	94.6
$\alpha$ His275 N $\epsilon$ –Ni(1)–L <sub>B</sub>	100.0	93.4
L <sub>B</sub> –Ni(1)–L <sub>1</sub>	63.2	69.7
L <sub>1</sub> –Ni(1)– $\alpha$ His249 N $\delta$	90.9	85.9
$\alpha$ His249 N $\delta$ –Ni(1)–L <sub>B</sub>	152.0	148.6
$\alpha$ His275 N $\epsilon$ –Ni(1)–L <sub>1</sub>	144.9	142.8
$\alpha$ Lys220* O02–Ni(2)– $\alpha$ His137 N $\epsilon$	92.4	94.7
$\alpha$ Lys220* O02–Ni(2)– $\alpha$ His139 N $\epsilon$	92.5	89.2
$\alpha$ Lys220* O02–Ni(2)–L <sub>2</sub>	92.2	92.5
$\alpha$ Lys220* O02–Ni(2)–L <sub>B</sub>	95.2	100.0
$\alpha$ Asp363 O $\delta$ 1–Ni(2)– $\alpha$ His137 N $\epsilon$	83.0	84.2
$\alpha$ Asp363 O $\delta$ 1–Ni(2)– $\alpha$ His139 N $\epsilon$	85.1	82.7
$\alpha$ Asp363 O $\delta$ 1–Ni(2)–L <sub>2</sub>	93.7	91.2
$\alpha$ Asp363 O $\delta$ 1–Ni(2)–L <sub>B</sub>	89.7	89.2
L <sub>2</sub> –Ni(2)–L <sub>B</sub>	62.1	68.1
L <sub>B</sub> –Ni(2)– $\alpha$ His137 N $\epsilon$	96.2	95.0
$\alpha$ His137 N $\epsilon$ –Ni(2)– $\alpha$ His139 N $\epsilon$	111.1	109.7
$\alpha$ His139 N $\epsilon$ –Ni(2)–L <sub>2</sub>	90.0	86.2
$\alpha$ Lys220* O02–Ni(2)– $\alpha$ Asp363 O $\delta$ 1	173.6	170.8
L <sub>B</sub> –Ni(2)– $\alpha$ His139 N $\epsilon$	151.3	152.8
L <sub>2</sub> –Ni(2)– $\alpha$ His137 N $\epsilon$	158.2	162.6
Ni(1)–L <sub>B</sub> –Ni(2)	122.6	115.7

[a] L<sub>1</sub>, L<sub>2</sub> indicate the ligand atom bound to Ni(1) and Ni(2), respectively, while L<sub>B</sub> indicates the Ni-bridging ligand atom. [b] Data taken from ref. [24].

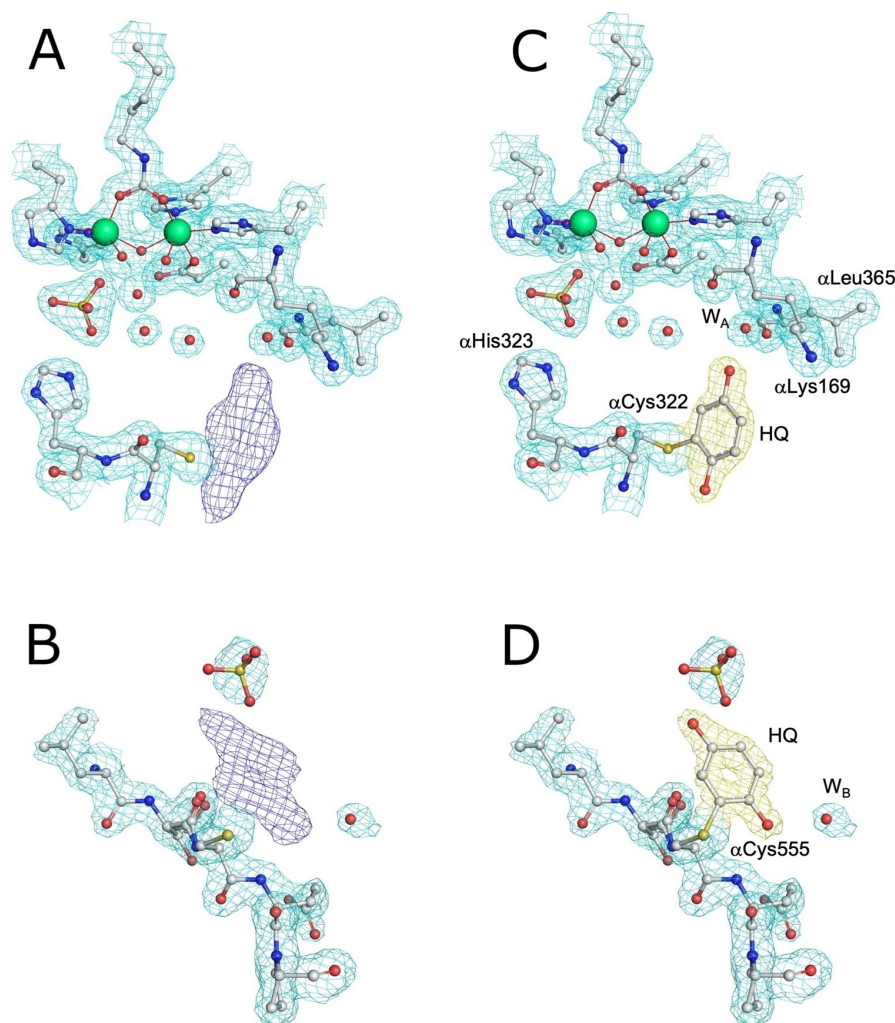


**Figure 2.** X-ray crystal structure of SPU bound to HQ A) in the active site region and B) in proximity to  $\alpha$ Cys555. The protein atomic models, nickel ions and solvent molecules are shown superimposed onto the final  $2F_o - F_c$  electron density map, contoured at  $1\sigma$  and colored gray. The unbiased  $F_o - F_c$  omit electron density maps for the ligands are shown contoured at  $3\sigma$  and colored blue. In C) and D) the same environments are presented showing the modeled HQ moieties superimposed onto the final  $2F_o - F_c$  electron density map, contoured at  $1\sigma$  and colored yellow. Carbon, nitrogen, oxygen, sulfur, and nickel are shown in gray, blue, red, yellow, and green, respectively.

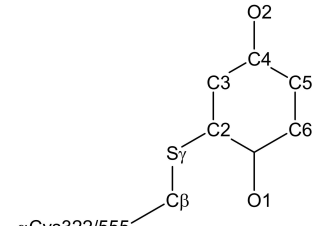
was already reported to be reactive towards BQ and  $\text{Au}^{\text{I}}$ .<sup>[29]</sup> These densities were successfully modeled as a hydroquinone moiety (Figure 2C,D) featuring a covalent bond between one of its aromatic C atoms (C2 following numbering reported in Table 4) and the  $S_{\gamma}$  atom of the corresponding Cys residue, with a conserved C–S distance of 1.7 Å (see Table 4 for a complete list of distances and angles). Regarding the HQ bound to  $\alpha$ Cys322, one hydroxy group points towards the  $\text{Ni}^{\text{II}}$  ions, similarly to what previously described for *p*-BQ,<sup>[24]</sup> CAT<sup>[26]</sup> and its derivatives<sup>[27]</sup> (with the exception of 3,6DMC). The orientation of both the HQ moieties bound to SPU in the present structure is the same as that found in the structure of SPU co-crystallized in the presence of *p*-BQ.

A significant difference between the reactivity of the two solvent-exposed Cys residues in urease ( $\alpha$ Cys322 and  $\alpha$ Cys555) emerges by comparing the structures of SPU bound to HQ (obtained upon co-crystallization of the protein either with HQ

or with *p*-BQ) and CAT and its derivatives: HQ and *p*-BQ bind both cysteines, while catechol-based inhibitors bind specifically the active site  $\alpha$ Cys322, leaving  $\alpha$ Cys555 free and not reacted. An obvious difference between the two cysteine residues is the presence of an adjacent histidine in the case of  $\alpha$ Cys322 ( $\alpha$ His323), but a possible role of the latter in determining the distinctive reactivity of the nearby cysteine towards (hydro)quinones and catechols is currently unclear.

An analysis of the hydrogen bond network between the hydroxyl O atoms of the two HQ moieties found bound to SPU and the surrounding water molecules has been performed. In the case of  $\alpha$ Cys322, the O atom in the *meta* position with respect to the thiol substituent (O2 following scheme in Table 4) points towards the entrance of the active site channel, forming a hydrogen bond with a water molecule ( $W_A$ , at 2.7 Å) that is also stabilized by two hydrogen bonds with  $\alpha$ Leu365 O and  $\alpha$ Lys169 O, both at 2.7 Å. No hydrogen bonds involving the

**Table 4.** Selected distances and angles in the SPU structure bound to HQ. Atom numbering follows the reported scheme. As a comparison, the same distances and angles for the structure of SPU co-crystallized in the presence of *p*-BQ (PDB ID: 5F5E) is reported.

	8A18 (HQ)	5F5E ( <i>p</i> -BQ) <sup>[a]</sup>
		
Distances [Å]		
C1–αCys322 Sγ	2.7	2.8
C2–αCys322 Sγ	1.7	1.6
C3–αCys322 Sγ	2.7	2.6
C4–αCys322 Sγ	4.0	3.9
C5–αCys322 Sγ	4.5	4.5
C6–αCys322 Sγ	4.0	4.0
O1–αCys322 Sγ	3.0	3.2
O2–αCys322 Sγ	5.1	5.0
C1–αCys555 Sγ	2.8	2.8
C2–αCys555 Sγ	1.8	1.7
C3–αCys555 Sγ	2.7	2.7
C4–αCys555 Sγ	4.1	4.1
C5–αCys555 Sγ	4.6	4.6
C6–αCys555 Sγ	4.1	3.9
O1–αCys555 Sγ	3.2	3.1
O2–αCys555 Sγ	5.1	4.9
Angles and torsion angles [°]		
C1–C2–αCys322 Sγ	119.8	124.7
C2–αCys322 Sγ–αCys322 Cβ	100.3	99.0
αCys322 Sγ–C2–C3	118.6	116.5
C1–C2–αCys322 Sγ–αCys322 Cβ	111.4	109.1
αCys322 Cβ–αCys322 Sγ–C2–C3	–66.8	–80.2
O1–C1–C2–αCys322 Sγ	0.8	9.7
C1–C2–αCys555 Sγ	125.7	128.6
C2–αCys555 Sγ–αCys555 Cβ	105.1	109.5
αCys555 Sγ–C2–C3	117.5	112.8
C1–C2–αCys555 Sγ–αCys555 Cβ	–105.4	–97.6
αCys322 Cβ–αCys322 Sγ–C2–C3	72.0	80.3
O1–C1–C2–αCys555 Sγ	–0.3	–1.4

[a] Data taken from ref. [24].

O atom in the ortho position with respect to the thiol substituent (O1 following scheme in Table 4) are detectable. In the case of αCys555, the O2 atom is at bond distance from an O atom of a sulfate ion present on the enzyme surface, while the O1 atom is at bond distance ( $W_B$ , 2.8 Å) from an ordered water molecule.

The final redox state of the moieties bound to αCys322 and αCys555 has been analyzed by a comparison of the C1–C2–Sγ–Cβ torsion angle values measured in the present ligand–cysteine adduct with the previously reported structure of SPU co-crystallized in the presence of the fully oxidized *p*-BQ (Table 4). The value of about 110° for both experimentally determined structures is strongly consistent with DFT calculations<sup>[24]</sup> and supports the presence of the fully reduced hydroquinone form bound to both cysteine residues. The described structural results obtained for the inactivation of

urease by HQ can be extended to MHQ, and tBHQ as will be further discussed in this work based on the kinetic results.

The kinetic characterization of urease inhibition by HQ, MHQ, and tBHQ was carried out by pre-incubating JBU with different concentrations of each inhibitor (in the range 0.2–6.4 mM) in the absence of substrate and monitoring the residual enzyme activity over increasing pre-incubation time periods upon substrate addition. The use of JBU for the kinetic measurements in place of SPU is justified by the fact that JBU does not require Na<sub>2</sub>SO<sub>3</sub> as a preservative to be maintained in an active form,<sup>[31]</sup> the presence of sulfite is indeed known to perturb the reactivity of both *p*-BQ<sup>[24]</sup> and CAT.<sup>[26]</sup> The results presented in Figure 3 show, for HQ, MHQ, and tBHQ, a time-dependent urease inhibition profile that follows a biphasic behavior, with an initial lag phase, whose extent decreases as the inhibitor concentration increases, followed by a faster reduction of enzyme activity eventually yielding its complete abolishment. These inhibition profiles resemble those previously observed for the inhibition of JBU by catechol<sup>[26]</sup> and its derivatives,<sup>[27]</sup> thus suggesting that HQ, MHQ and tBHQ inhibit urease with an analogous mechanism; these curves differ from those previously reported for the urease inhibition by the fully oxidized *p*-BQ<sup>[24]</sup> for which the experimental data were successfully fitted to a single exponential decay with a time constant  $k_{app}$  [s<sup>–1</sup>] linearly dependent on the concentration of *p*-BQ. Such behavior for *p*-BQ, corroborated by the structural details obtained from crystallographic data, was rationalized with the formation of a covalent adduct on the reactive αCys322 residue belonging to the active site mobile flap, an irreversible process of the first kinetic order with respect both urease and ligand that eventually leads to an inactive form of the enzyme. Even though these inhibition profiles are peculiar for irreversible enzyme inactivators forming stable covalent adducts with essential functional groups of the enzyme,<sup>[38]</sup> the much greater concentration range in which HQ, MHQ and tBHQ behave as effective inhibitors of urease with respect to *p*-BQ (at least one order of magnitude), together with the aforementioned similarity of the kinetic data with those reported for catechols, directed our attention to the possibility that HQ, MHQ and tBHQ share with catechols the same mechanism governing urease inactivation, namely an autocatalytic radical-based mechanism that involves the formation of a semiquinone radical upon oxidation of the starting compound by dissolved O<sub>2</sub> in solution. The presence of a lag phase (although limited to a few minutes) in the case of urease inhibition by catechol and hydroquinone might represent a challenge to be overcome, as it is desirable to develop inhibitors with minimal (or no) lag phase in the onset of inhibition.<sup>[39]</sup>

The kinetic data were then analyzed by performing a simultaneous global fit using the following Equation (1), originally derived to kinetically characterize the inhibition of urease by catechol:<sup>[26]</sup>

$$[JBU_{act}] = [JBU_{act}]_0 \exp(-k_1 t - k_2 t^2) \quad (1)$$

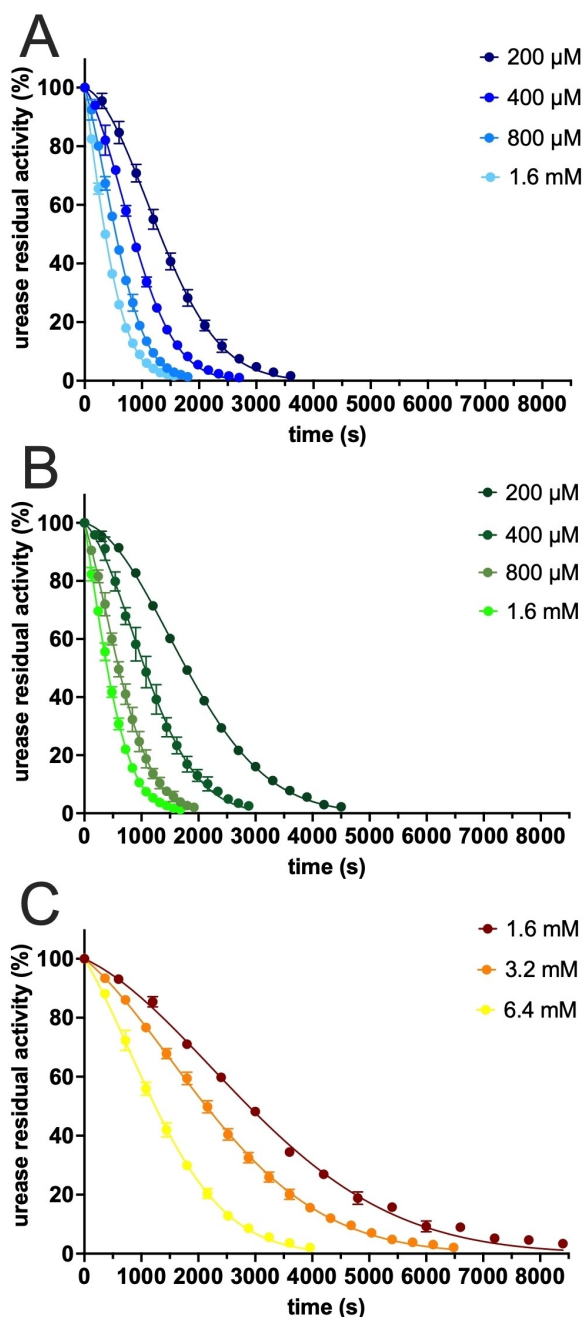
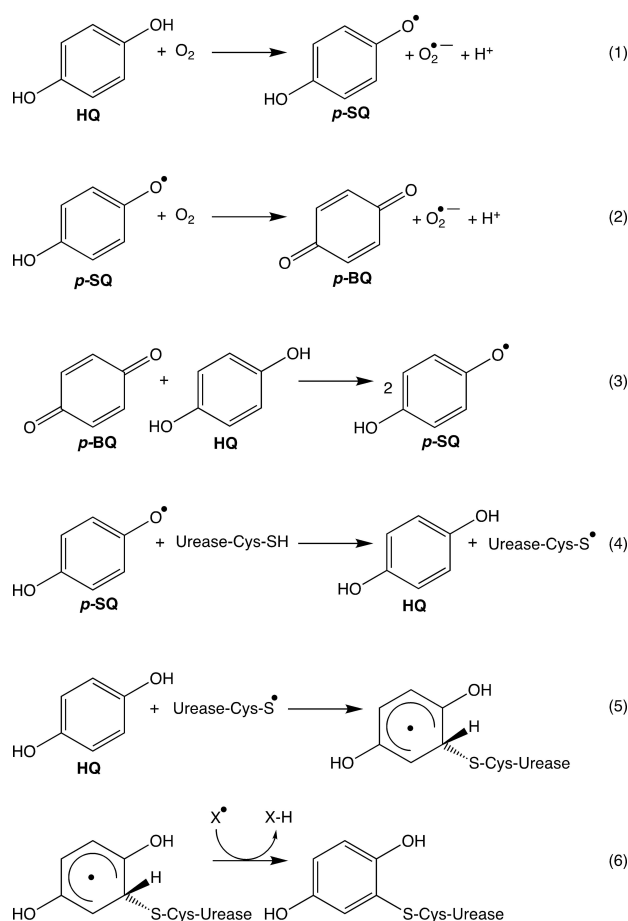


**Figure 3.** Plots of JBU residual activity vs. time of incubation at different concentrations of A) HQ, B) MHQ, and C) *t*BHQ. The lines represent the result of the global fits of the data obtained from Equation (1).

In this equation, the  $k_1$  and  $k_2$  constants are functions of the single kinetic constants that regulate each step of the inactivation mechanism as well as the concentration of the inhibitor (Scheme 1). In order to quantitatively compare the inhibition strengths of HQ, MHQ, and *t*BHQ, the values of the  $k_1 \cdot k_2$  products determined for the data collected at a single and shared inhibitor concentration (1.6 mM) are reported in Table 5, as already done for catechol and its mono- and di-methyl derivatives.<sup>[26,27]</sup> The resulting analysis showed that the inactivation proficiency of the hydroquinone derivatives follows the



**Scheme 1.** Working hypothesis for the mechanism of inactivation of urease by hydroquinones.

**Table 5.** Kinetic parameters for inhibition of JBU by 1.6 mM HQ, MHQ and *t*BHQ.

	Compound @1.6 mM		
	HQ	MHQ	<i>t</i> BHQ
$k_1$	$1.55 \times 10^{-3}$	$1.33 \times 10^{-3}$	$0.0902 \times 10^{-3}$
$k_2$	$1.07 \times 10^{-6}$	$1.01 \times 10^{-6}$	$5.21 \times 10^{-6}$
$k_1 \cdot k_2 (\times 10^{10})$	16.6	13.4	0.0470

order  $\text{HQ} \approx \text{MHQ} > \text{tBHQ}$ . This trend can be at least partially ascribed to the increased steric hindrance of the *tert*-butyl groups of *t*BHQ, as compared to the smaller methyl group of MHQ and the plain HQ, that would render the entrance of *t*BHQ in the active site channel and the subsequent interaction of the active species with  $\alpha\text{Cys322}$  less favorable.

While such a comparison of  $k_1 \cdot k_2$  products was possible within the HQ, MHQ, and *t*BHQ triad, a similar quantitative assessment of the relative urease inhibition efficiency between catechols and hydroquinones cannot be carried out because of the much lower inhibition efficiency of the latter, which prevents the possibility to perform the experiments in the same range of concentrations for the two classes of compounds. However, a qualitative comparison was carried out by evaluating the concentration required to achieve a 50% decrease of

urease activity in a range of  $10^2$ – $10^3$  seconds: such an inhibition level is achieved at 20  $\mu\text{M}$  by catechols,<sup>[26–27]</sup> and 1.6 mM by hydroquinones, reflecting an overall approximately two orders of magnitude greater inhibition efficiency of the former with respect to the latter.

The overall higher reactivity of catechols can be rationalized on the basis of the different reduction potentials for the oxidized/semireduced/reduced forms of the two classes of compounds:<sup>[40]</sup> assuming that the same radical-based autocatalytic multistep urease inactivation mechanism is operational in both cases (Scheme 1), the starting reduced forms must undergo a one-electron oxidation step in order for the active species, namely their corresponding semiquinone moieties, to be generated. The one-electron oxidation of HQ to  $p\text{-SQ}^{\bullet-}$  is more favorable than that of CAT to  $o\text{-SQ}^{\bullet-}$  (with reduction potentials of the semiquinone forms equal to +473 and +530 mV, respectively). However, in both cases the  $\text{SQ}^{\bullet-}$  species tends to undergo a disproportionation event to yield the fully reduced (HQ or CAT) and the fully oxidized ( $p\text{-BQ}$  or  $o\text{-BQ}$ ) moieties. This disproportionation is more favorable in the case of HQ than in the case of CAT (with reduction potentials equal to +374 mV and +320 mV, respectively), resulting in values for the corresponding equilibrium constants of  $2.2 \times 10^6$  and  $2.5 \times 10^5$ , respectively. Overall, this process causes a smaller concentration of the reactive semiquinone species in the case of HQ as compared to CAT, which in turn could rationalize the reduced reactivity of HQ (and, consequently, of its methyl and *tert*-butyl derivatives) against urease with respect to their *ortho* analogues.

## Conclusions

The molecular details of urease inactivation by hydroquinone and its methyl and *tert*-butyl derivatives have been elucidated by using macromolecular X-ray crystallography and kinetic studies. The inactivation process is consistent with a radical-based mechanism that leads to the formation of a covalent adduct between hydroquinones and the conserved  $\alpha\text{Cys322}$  located on the catalytic mobile flap, blocking the flap in the open conformation and inactivating the enzyme. The high conservation of the mobile flap cysteine in ureases expressed by ureolytic bacteria renders this residue a key target for the development of novel urease inhibitors based on polyhydroxylated aromatic molecules by structure-based design and structure–activity relationship studies, with potentially very high benefits both for medicine and the agro-environment.

## Acknowledgements

This research was partially supported by CIRMMMP (Consorzio Interuniversitario di Risonanze Magnetiche di Metallo Proteine) and the University of Bologna. X-ray diffraction data were collected at the PETRA III storage ring operated by EMBL Hamburg (DESY, Hamburg, Germany; beam time award number

MX-720). We thank the facility for the allocated beam time and technical support.

## Acknowledgements

Open Access funding provided by Università degli Studi di Bologna within the CRUI-CARE Agreement.

## Conflict of Interest

The authors declare no conflict of interest.

## Data Availability Statement

The data that support the findings of this study are available from the corresponding author upon reasonable request.

**Keywords:** enzyme inhibition · hydroquinones · nickel · protein crystallography · urease

- [1] F. R. Krueger, W. Werther, J. Kissel, E. R. Schmid, *Rapid Commun. Mass Spectrom.* **2004**, *18*, 103–111.
- [2] a) B. L. Trumpower, *J. Biol. Chem.* **1990**, *265*, 11409–11412; b) R. Stocker, V. W. Bowry, B. Frei, *Proc. Natl. Acad. Sci. USA* **1991**, *88*, 1646–1650.
- [3] R. Tiemann, G. Renger, P. Graber, H. T. Witt, *Biochim. Biophys. Acta* **1979**, *546*, 498–519.
- [4] B. A. G. de Melo, F. L. Motta, M. H. A. Santana, *Mater. Sci. Eng. C* **2016**, *62*, 967–974.
- [5] K. A. Thorn, J. B. Arterburn, M. A. Mikita, *Environ. Sci. Technol.* **1992**, *26*, 107–116.
- [6] R. H. Thomson, *Naturally Occurring Quinones*, Elsevier, **2012**, p. 734.
- [7] a) L. Van Puyvelde, J. Bosselaers, C. Stevens, N. De Kimpe, J. Van Gestel, P. Van Damme, *J. Agric. Food Chem.* **1999**, *47*, 2116–2119; b) J. R. Vyvyan, *Tetrahedron* **2002**, *58*, 1631–1646.
- [8] a) K. N. Raymond, G. Müller, B. F. Matzanke, *Struct. Chem.*, Springer, Berlin, Heidelberg, **1984**, pp. 49–102; b) S. Deiana, C. Gessa, M. Marchetti, M. Usai, *Soil Sci. Soc. Am. J.* **1995**, *59*, 1301–1307.
- [9] A. P. DeCaprio, *Crit. Rev. Toxicol.* **1999**, *29*, 283–330.
- [10] K. A. Arndt, T. B. Fitzpatrick, *Jama* **1965**, *194*, 965–967.
- [11] J. O'Donoghue, *Official J. Eur. Commun.* **2000**, *56*, 42–46.
- [12] W. Westerhof, T. J. Kooyers, *J. Cosmet. Dermatol.* **2005**, *4*, 55–59.
- [13] C. Siegers, J. Siegers, R. Pentz, C. Budinet, J. Freudenstein, *Pharmac. Pharmacol. Lett.* **1997**, *7*, 90–92.
- [14] a) A. L. Odom, C. A. Hatwig, J. S. Stanley, A. M. Benson, *Biochem. Pharmacol.* **1992**, *43*, 831–836; b) C. E. Myers, W. P. McGuire, R. H. Liss, I. Ifrim, K. Grotzinger, R. C. Young, *Science* **1977**, *197*, 165–167; c) B. Kalyanaraman, K. M. Morehouse, R. P. Mason, *Arch. Biochem. Biophys.* **1991**, *286*, 164–170.
- [15] a) J. M. Bremner, L. A. Douglas, *Soil Biol. Biochem.* **1971**, *3*, 297–307; b) L. G. Bundy, J. M. Bremner, *Soil Biol. Biochem.* **1973**, *5*, 847–853; c) J. M. Bremner, R. L. Mulvaney, in *Urease Activity in Soils* (Ed.: R. G. Burns), Academic Press, New York, **1978**, pp. 149–196; d) R. L. Mulvaney, J. M. Bremner, *Soil Biol. Biochem.* **1978**, *10*, 297–302; e) W. Zaborska, M. Kot, K. Superata, *J. Enzyme Inhib. Med. Chem.* **2002**, *17*, 247–253; f) W. Zaborska, B. Krajewska, M. Kot, W. Karcz, *Bioorg. Chem.* **2007**, *35*, 233–242; g) M. Kot, W. Zaborska, *J. Enzyme Inhib. Med. Chem.* **2006**, *21*, 537–542; h) B. Krajewska, *J. Mol. Catal. B* **2009**, *59*, 9–21.
- [16] a) M. J. Maroney, S. Ciurli, *Chem. Rev.* **2014**, *114*, 4206–4228; b) L. Mazzei, F. Musiani, S. Ciurli, in *Urease* (Eds.: D. Zamble, M. Rowińska-Zyrek, H. Kozłowski), Royal Society of Chemistry, **2017**, pp. 60–97; c) L. Mazzei, F. Musiani, S. Ciurli, *J. Biol. Inorg. Chem.* **2020**, *25*, 829–845.
- [17] a) R. P. Hausinger, *Microbiol. Rev.* **1987**, *51*, 22–42; b) H. L. Mobley, R. P. Hausinger, *Microbiol. Rev.* **1989**, *53*, 85–108.



- [18] a) R. L. Blakeley, J. A. Hinds, H. E. Kunze, E. C. Webb, B. Zerner, *Biochemistry* **1969**, *8*, 1991–2000; b) N. E. Dixon, P. W. Riddles, C. Gazzola, R. L. Blakeley, B. Zerner, *Can. J. Biochem.* **1980**, *58*, 1335–1344; c) L. Mazzei, S. Ciurli, in *Urease*, Wiley, Chichester, **2021**, pp. 1–17.
- [19] J. C. Rutherford, *PLoS Pathog.* **2014**, *10*, e1004062.
- [20] S. Kiss, M. Simihaian, *Improving Efficiency of Urea Fertilizers by Inhibition of Soil Urease Activity*, Kluwer Academic, Dordrecht, **2002**, p. 417.
- [21] a) B. Marshall, J. R. Warren, *Lancet* **1984**, *323*, 1311–1315; b) P. Bauerfeind, R. Garner, B. E. Dunn, H. L. T. Mobley, *Gut* **1997**, *40*, 25–30; c) K. Stingl, K. Altendorf, E. P. Bakker, *Trends Microbiol.* **2002**, *10*, 70–74; d) C. Zhou, F. Bhinderwala, M. K. Lehman, V. C. Thomas, S. S. Chaudhari, K. J. Yamada, K. W. Foster, R. Powers, T. Kielian, P. D. Fey, *PLoS Pathog.* **2019**, *15*, e1007538; e) A. H. Gordon, P. D. Hart, M. R. Young, *Nature* **1980**, *286*, 79–80; f) D. L. Clemens, B. Y. Lee, M. A. Horwitz, *J. Bacteriol.* **1995**, *177*, 5644–5652; g) W. Lin, V. Mathys, Y. Ang Emily Lei, Q. Koh Vanessa Hui, M. Martínez Gómez Julia, T. Ang Michelle Lay, Z. Zainul Rahim Siti, P. Tan Mai, K. Pethe, S. Alonso, J. L. Flynn, *Infect. Immun.* **2012**, *80*, 2771–2779; h) G. Young, D. Amid, V. Miller, *J. Bacteriol.* **1996**, *178*, 6487–6495; i) G. M. Cox, J. Mukherjee, G. T. Cole, A. Casadevall, J. R. Perfect, *Infect. Immun.* **2000**, *68*, 443–448.
- [22] WHO in *Global Priority List of Antibiotic-Resistant Bacteria To Guide Research, Discovery, and Development of New Antibiotics*, **2017**.
- [23] F. Paulot, D. J. Jacob, *Environ. Sci. Technol.* **2014**, *48*, 903–908.
- [24] L. Mazzei, M. Cianci, F. Musiani, S. Ciurli, *Dalton Trans.* **2016**, *45*, 5455–5459.
- [25] a) S. Benini, W. R. Rypniewski, K. S. Wilson, S. Miletti, S. Ciurli, S. Mangani, *Structure* **1999**, *7*, 205–216; b) S. Benini, M. Cianci, L. Mazzei, S. Ciurli, *J. Biol. Inorg. Chem.* **2014**, *19*, 1243–1261; c) L. Mazzei, M. Cianci, U. Contaldo, F. Musiani, S. Ciurli, *Biochemistry* **2017**, *56*, 5391–5404; d) L. Mazzei, M. Cianci, S. Benini, S. Ciurli, *Angew. Chem. Int. Ed.* **2019**, *58*, 7415–7419; *Angew. Chem.* **2019**, *131*, 7493–7497; e) L. Mazzei, M. Cianci, U. Contaldo, S. Ciurli, *J. Agric. Food Chem.* **2019**, *67*, 2127–2138; f) L. Mazzei, M. Cianci, S. Benini, S. Ciurli, *Chem. Eur. J.* **2019**, *25*, 12145–12158.
- [26] L. Mazzei, M. Cianci, F. Musiani, G. Lente, M. Palombo, S. Ciurli, *J. Inorg. Biochem.* **2017**, *166*, 182–189.
- [27] L. Mazzei, U. Contaldo, F. Musiani, M. Cianci, G. Bagnolini, M. Roberti, S. Ciurli, *Angew. Chem. Int. Ed.* **2021**, *60*, 6029–6035; *Angew. Chem.* **2021**, *133*, 6094–6100.
- [28] a) L. Mazzei, D. Cirri, M. Cianci, L. Messori, S. Ciurli, *J. Inorg. Biochem.* **2021**, *218*, 111375–111383; b) L. Mazzei, M. Cianci, A. Gonzalez Vara, S. Ciurli, *Dalton Trans.* **2018**, *47*, 8240–8247.
- [29] a) L. Mazzei, L. Massai, M. Cianci, L. Messori, S. Ciurli, *Dalton Trans.* **2021**, *50*, 14444–14452; b) L. Mazzei, M. N. Wenzel, M. Cianci, M. Palombo, A. Casini, S. Ciurli, *ACS Med. Chem. Lett.* **2019**, *10*, 564–570.
- [30] C. Tarsia, A. Danielli, F. Florini, P. Cinelli, S. Ciurli, B. Zambelli, *Biochim. Biophys. Acta Gen. Subj.* **2018**, *1862*, 2245–2253.
- [31] L. Mazzei, M. Cianci, S. Benini, L. Bertini, F. Musiani, S. Ciurli, *J. Inorg. Biochem.* **2016**, *154*, 42–49.
- [32] S. Benini, C. Gessa, S. Ciurli, *Soil Biol. Biochem.* **1996**, *28*, 819–821.
- [33] M. Cianci, G. Bourenkov, G. Pompidor, I. Karpics, J. Kallio, I. Bento, M. Roessele, F. Cipriani, S. Fiedler, T. R. Schneider, *J. Synchrotron Radiat.* **2017**, *24*, 323–332.
- [34] W. Kabsch, *Acta Crystallogr. D Biol. Crystallogr.* **2010**, *66*, 125–132.
- [35] a) P. Evans, *Acta Crystallogr. D Biol. Crystallogr.* **2006**, *62*, 72–82; b) P. R. Evans, *Acta Crystallogr. D Biol. Crystallogr.* **2011**, *67*, 282–292.
- [36] G. N. Murshudov, A. A. Vagin, E. J. Dodson, *Acta Crystallogr. D Biol. Crystallogr.* **1997**, *53*, 240–255.
- [37] a) P. Emsley, K. Cowtan, *Acta Crystallogr. D Biol. Crystallogr.* **2004**, *60*, 2126–2132; b) P. Emsley, B. Lohkamp, W. G. Scott, K. Cowtan, *Acta Crystallogr. D Biol. Crystallogr.* **2010**, *66*, 486–501.
- [38] R. B. Silverman, in *Mechanism-Based Enzyme Inactivators*, Vol. 249, Academic Press, New York, **1995**, pp. 240–283.
- [39] A. Kandale, K. Patel, W. M. Hussein, S. J. Wun, S. Zheng, L. Tan, N. P. West, G. Schenk, L. W. Guddat, R. P. McGeary, *J. Med. Chem.* **2021**, *64*, 1670–1684.
- [40] Y. Song, G. R. Buettner, *Free Radical Biol. Med.* **2010**, *49*, 919–962.
- [41] M. D. Winn, C. C. Ballard, K. D. Cowtan, E. J. Dodson, P. Emsley, P. R. Evans, R. M. Keegan, E. B. Krissinel, A. G. Leslie, A. McCoy, S. J. McNicholas, G. N. Murshudov, N. S. Pannu, E. A. Potterton, H. R. Powell, R. J. Read, A. Vagin, K. S. Wilson, *Acta Crystallogr. D Biol. Crystallogr.* **2011**, *67*, 235–242.
- [42] D. W. Cruickshank, *Acta Crystallogr. D Biol. Crystallogr.* **1999**, *55*, 583–601.

Manuscript received: June 9, 2022

Accepted manuscript online: August 22, 2022

Version of record online: September 22, 2022